Investigation of new particle formation at the summit of Mt. Tai, China

Ganglin Lv[1], Xiao Sui[1], Jianmin Chen[1,2*], Rohan Jayaratne[3], Abdelwahid Mellouki[1,4]

[1]School of Environmental Science and Engineering, Environment Research Institute, Shandong University, Jinan, Shandong 250100, China

[2]Shanghai Key Laboratory of Atmospheric Particle Pollution and Prevention (LAP3), Institute of Atmospheric Sciences, Fudan University, Shanghai 200433, China

[3]International Laboratory for Air Quality and Health, Science and Engineering Faculty, Queensland University of Technology, GPO Box 2434, Brisbane QLD 4001, Australia

[4]Institut de Combustion, Aérothermique, Réactivité et Environnement, CNRS, 45071 Orléans cedex 02, France

Correspondence to: Jianmin Chen (jmchen@fudan.edu.cn); Tel.: +86 53188363711; fax: +86 531 88361990

Abstract. To date few comprehensive field observations of new particle formation (NPF) have been carried out at mountain-top sites in China. In this study, simultaneous measurements of particle size distribution, trace gases, meteorological parameters, mass concentration and chemical composition of $PM_{2.5}$ were performed at the summit of Mt. Tai (1534 m ASL) from 25 July to 24 August 2014 (Phase I), 21 September to 9 December 2014 (Phase II), and 16 June to 7 August 2015 (Phase III), to investigate the characteristics and favorable conditions of NPF in a relatively clean mountain-top environment. The NPF events were identified based on the particle size distribution, and 66 such events were observed in a period of 164 days — corresponding to an occurrence frequency of 40%. The formation rates of 3 nm particles (J_3) and growth rates (GR) were in the ranges of 0.82-25.04 cm^{-3} s^{-1} and 0.58-7.76 nm h^{-1}, respectively. On average, the condensation sink (CS), O_3 concentration, air temperature and relative humidity were lower, whereas the SO_2 concentration was higher on NPF days than on non-NPF days. Factors of trace gases, meteorological conditions and air mass transport were mainly through affecting sinks and sources in determining the NPF events. Three categories of backward trajectories were classified in the study, among which continental air mass was the majority. The continental air masses passing through more polluted areas (denoted as Type I) could enhance the occurrence of NPF, which was possibly associated with high level of precursors carried from the polluted regions. In addition, maritime air mass seemed not to be favorable condition for NPF because of potential lack of precursors.

Keywords. New particle formation; Mountain observations; Favorable conditions; sinks and sources

1 Introduction

Atmospheric aerosols play a critical role in affecting global radiation forcing and climate (Kazil et al., 2010), directly through scattering and absorption of solar radiation, and indirectly by modifying cloud properties and lifetimes as the potential cloud condensation nuclei (CCN) (Kuang et al., 2010). Aerosol particles are also involved in several atmospheric chemistry processes such as enhancing haze and decreasing visibility, which is associated with the air quality (Guo et al., 2014). In addition, aerosol particles can harm human health by inhalation (Han, 2012;Butt et al., 2016). Previous studies have shown that the nucleation of atmospheric gas-phase precursors and the subsequent growth to larger particles, widely known as new particle formation (NPF), is the largest source of atmospheric aerosol particles (Zhang et al., 2012). Field observations have exhibited that NPF typically increase the particle number concentration by a factor of two to ten (Gong et al., 2010). Modeling studies also revealed that NPF accounted for 5-50% of CCN in the lower boundary layer (Spracklen et al., 2008). An in-depth study of the process of NPF and its effects could help control atmospheric aerosol pollution in China.

With the development of instruments that measure particle size distribution, NPF events have been widely observed all over the world in recent decades. These observation sites include northern-most sub-arctic, remote boreal forests, industrialized agricultural regions, high-iodine coastal environments, and polluted urban areas (Dal Maso et al., 2002). The frequency of NPF events varies significantly between locations. Hallar et al. (2011) reported that NPF events in urban areas, such as Pittsburgh, USA occurred on about 35-50% of all days, whereas the corresponding values at the remote background sites in Finland and Sweden were just 2-27%. Manninen et al. (2010) found that the frequency of NPF events ranged from 21% to 57% at the twelve field sites around Europe, and the number of observed NPF days was closely related to the regional atmospheric conditions.

In the past decade, many campaigns and studies on NPF have been carried out in China. NPF events were first reported in China in 2004 by Wehner et al. (2004) who used a Twin Differential Mobility Particle Sizer (TDMPS). Soon after, Liu et al. (2008) observed NPF at a rural/coastal site in XinKen (Guangdong Province). In 2005, Gao et al. (2009) investigated the occurrence of NPF in a suburban environment in the Yangtze River delta using a Wide-range Particle Spectrometer (WPS). Thereafter, several observations of NPF have been widely reported in urban, suburban and rural environments around China (An et al., 2015;Wang et al., 2011;Peng et al., 2014). However, there have not been many observations of NPF on the mountain-top sites in China. At the remote high elevation sites, the NPF revealed the specific characteristics. Lots of mountain studies of NPF ranged around the world so far, such as Mount Norikura in Japan, Jungfraujoch (3580 m asl) in Switzerland, Mt. Werner in America, and Himalayas in Nepal (Hallar et al., 2011;Chiharu et al., 2008;Weingartner et al., 1999;Venzac et al., 2008). In 2008, Zhang et al. (2016) firstly observed the occurrence of NPF in China on Mt. Huang (1840 m ASL) with a WPS instrument. However, these recent mountain-top studies in China had significant limitations in measurement methods and seasonal variations. Clearly, multi-seasonal observations by using nanometer-scale instruments

are essential and valuable for NPF research in mountain environments.

Particle formation and growth rates vary between different field environments. Kulmala et al. (2004), reviewing a number of studies, found that the typical formation rate was in the range of 0.01-10 cm^{-3} s^{-1}. In urban areas it may be about 100 cm^{-3} s^{-1}, while in coastal zones it can be as high as 10^4-10^5 cm^{-3} s^{-1}. Typical growth rate of newly formed particles ranges from 1 to 20 nm h^{-1}, and at some coastal areas it is as high as 200 nm h^{-1}.

Previous studies have shown that sulfuric acid, ammonia, organic vapors, and iodide species in the atmosphere were involved in the nucleation process under specific conditions. Gaseous sulfuric acid was the most critical candidate that participated in binary, ternary and ion induced nucleation (Boy et al., 2005;Wang et al., 2011;Zhang, 2010;Saunders et al., 2010;Allan et al., 2015). It has also been shown that the nucleation rate is a function of sulfuric acid concentration with a power dependency exponent, whose exponent varied significantly between different nucleation theories (Kulmala et al., 2006;Wang et al., 2011). However, the occurrence of NPF cannot be determined by sulfuric acid alone, and other factors such as pre-existing particles, meteorological conditions, and air mass transport should also be considered. Comprehensive investigations of these factors affecting the occurrence of NPF in China have mainly been conducted in urban/suburban/rural environments. Since the mechanisms of NPF under heavily polluted conditions is significantly different from that under relatively clean conditions (Kulmala et al., 2016;Hu et al., 2016;Wang et al., 2013), the comprehensive investigation of NPF on relatively clean mountain-top sites is of great important in China. In addition, favorable conditions to NPF events were characteristic of specific locations (Nie et al., 2014;Wang et al., 2014a;An et al., 2015), thus an intensive analysis for specific sites, such as Mt. Tai in this study, is also vital.

In this paper, we present the results of the intensive field observations at the summit of Mt. Tai (1534 m ASL), which is a relatively clean mountain-top environment. This study was based on simultaneous measurements of particle size distribution, meteorological parameters, gaseous species, mass concentration and chemical composition of $PM_{2.5}$ during three campaigns (25 July to 24 August 2014, Phase I; 21 September to 9 December 2014, Phase II; 16 June to 7 August 2015, Phase III). The general characteristics of NPF events were calculated on the basis of particle size distribution, besides condensation sinks (CS), sources, meteorological conditions, long-range air mass transport were mainly discussed to explore the factors affecting the occurrence of NPF.

2 Methods

2.1 Site description

The observations were conducted at the summit of Mt. Tai (36.25 °N, 117.1 °E, 1534 m ASL), located nearly the centre of Shandong Province, eastern China. Mt. Tai is one of the highest mountains near the East China Sea on the transport path of the Asian continental outflow (Li et al., 2011), adjacent to the Bohai Sea (B-S) and Yellow Sea (Y-S). The field site is just at

the summit of Mt. Tai, and its surroundings are dominated by dense vegetation and mountains with few anthropogenic sources. The nearest mid-size city, Tai'an with a population of 670,000, is located approximately 15 km away to the south and southeast. The city of Ji'nan (population: 2,800,000), capital of Shandong Province, is 60 km to the north. During daytime, the summit of Mt. Tai reaches close to the top of the planetary boundary layer (PBL), and the observation site is representative of the region (Zhang et al., 2014;Sun et al., 2016). All the instruments were installed inside a large trailer home, sampling through short inlet tubes outside the container at a height of about 3 m above the ground level.

2.2 Measurement techniques

Two types of particle size distribution instruments, namely neutral cluster and air ion spectrometer (NAIS) and wide-range particle spectrometer (WPS), two gas monitors (SO_2 and O_3), an instrument for mass concentration of $PM_{2.5}$ and a monitor for chemical composition in $PM_{2.5}$ were used in this study. In addition, meteorological parameters including air temperature (T), relative humidity (RH), wind speed (WS), wind direction (WD) and visibility were also recorded in real time.

The NAIS is a multichannel nanometer aerosol instrument which can measure the size distribution of aerosol particles and ions (charged particles and cluster ions) of both polarities simultaneously. The aerosol particle distribution of NAIS is in the size range of 2─40 nm, and the ion distribution is in the electric mobility range of 0.0013-3.2 $cm^2\ V^{-1}\ s^{-1}$ (equivalent to particle Millikan diameters of 0.8-40 nm). The instrument consists of two multichannel electrical mobility analyzer columns, one for each polarity. The aerosols are classified according to electrical mobility and measured with an array of twenty-one electrometers per column. In this study, the total time of each measurement cycle was set at 5 min, comprising of sampling intervals as follows: particles 120 s, ions 120 s and offset 60 s.

The WPS is a high-resolution aerosol spectrometer which combines a differential mobility analyzer (DMA), a condensation particle counter (CPC) and a laser light scattering (LPS). The diameter range of WPS was from 10 to 10,000 nm, and 48 channels were used in the DMA and 24 channels were used for the LPS. The scan time for the entire size range was set to 5 min.

The concentration of SO_2 in the atmosphere was measured with a pulsed ultraviolet fluorescence analyzer (Model 43C, Thermo Electron Corporation-TEC), and O_3 was measured with an ultraviolet photometric analyzer (Model 49C, TEC). Mass concentration of $PM_{2.5}$ was detected by a monitor utilizing a combination of beta attenuation and light scattering technology (Model 5030 SHARP Monitor, Thermo Fisher Scientific), and chemical composition of $PM_{2.5}$ was measured by a Monitor for Aerosols and Gases (MARGA, ADI20801, Applikon-ECN, Netherlands). Meteorological data were obtained in real time with an automatic meteorological station (MILOS520, Vaisala, Finland).

2.3 Data analysis

2.3.1 Formation rate, growth rate and condensation sink

In this study, particles in the size range of 3-20 nm was regarded as nucleation particles, and the formation rate of nucleation mode particles, $J_{3\text{-}20}$, can be expressed (Dal Maso et al., 2005) as:

$$J_{3\text{-}20} = \frac{dN_{3\text{-}20}}{dt} + F_{\text{CoagS}} + F_{\text{growth}} \quad (1)$$

where $dN_{3\text{-}20}/dt$ is the net rate of increased nucleation mode particles, F_{CoagS} is the coagulation loss and F_{growth} is the loss of particles growing out of size range. In our observation, the F_{growth} term could be neglected because particles growing beyond 20 nm before formation ended was relatively rare. In addition, the formation rate of 3 nm particles, J_3, was also calculated from the NAIS data (Sihto et al., 2006;Kulmala et al., 2012) by using equation (2):

$$J_3 = \frac{dN_{3\text{-}6}}{dt} + \text{CoagS}_{Dp=4\text{ nm}} \cdot N_{3\text{-}6} + \frac{1}{3\text{ nm}} \text{GR}_{3\text{-}6} \cdot N_{3\text{-}6} \quad (2)$$

where $\text{CoagS}_{DP=4\text{ nm}}$ represents the coagulation sink of 4 nm particles, an approximation for the interval of 3-6 nm particles. $\text{GR}_{3\text{-}6}$ and $N_{3\text{-}6}$ denote the particle growth rate and particle number concentration between 3 and 6 nm, respectively.

The particle growth rate, GR, was determined by the maximum concentration method (Kulmala et al., 2012):

$$\text{GR} = \frac{\Delta D_{\text{m}}}{\Delta t} = \frac{D_{\text{m2}} - D_{\text{m1}}}{t_2 - t_1} \quad (3)$$

where D_{m1} and D_{m2} are the geometric median diameters of representative particles at the start time t_1 and the end time t_2, respectively.

Condensation sink, CS, determines the rate of molecules condensing on the pre-existing aerosols, and it is given by equation (4) (Dal Maso et al., 2005;Kulmala et al., 2001):

$$\text{CS} = 2\pi D \sum_i \beta_{Mi} \, Dp_i \, N_i \quad (4)$$

where D is the diffusion coefficient for sulfuric acid, and β_{M} is the size-dependent transitional correction factor.

2.3.2 Sulfuric acid proxy

Direct measurement of gas-phase sulfuric acid concentration was not available in this study. Instead, the predictive proxy for sulfuric acid ($[H_2SO_4]$) could be roughly estimated based on the solar radiation (SR), SO_2 concentration, CS and RH (Mikkonen et al., 2011):

$$[H_2SO_4] = 8.21 \cdot 10^{-3} \cdot k \cdot \text{SR} \cdot [SO_2]^{0.62} \cdot (\text{CS} \cdot \text{RH})^{-0.13} \quad (5)$$

Here k is a temperature-dependent reaction rate constant, and the solar radiation is estimated from Hybrid Single Particle Lagrangian Integrated Trajectory (HYSPLIT) Model developed by the Air Resources Laboratory of U.S. National Oceanic and Atmospheric Administration (NOAA). The absolute values of sulfuric acid concentration contain some error with the real concentrations because of great uncertainty of solar radiation from HYSPLIT, but its diurnal variation pattern is acceptable.

3 Results and discussion

3.1 Classification and characteristics of the NPF events

Basically, an NPF event could be defined as a distinct burst of new nucleation mode particles and subsequent growth of particles to larger size over a period of time (Dal Maso et al., 2005;Hallar et al., 2011;Wang et al., 2014a;Xiao et al., 2015). For the Mt. Tai observations in this study, neutral particles generally account1ed for more than 95% of the total particles during NPF events, so a detailed discussion of ions will not be the focus in this paper.

The data presented in this study covered three campaigns from 25 July to 24 August 2014 (Phase I), 21 September to 9 December 2014 (Phase II), and 16 June to 7 August 2015 (Phase III) at the summit of Mt. Tai. Observations over 164 days showed that the NPF events occurred on 66 days, corresponding to an occurrence frequency of 40%. NPF events were observed throughout the measurement campaigns with a highest occurrence frequency of 56% during Phase II (during the other two Phases the average frequency was only 21%). The difference may be attributed to the rainy/foggy conditions that prevailed during the Phases I and III which hindered the NPF.

In this study, we defined the observed start time of NPF events based on the significant enhancement of particle number concentration between 3 and 6 nm, $N_{3\text{-}6}$. The analysis showed that approximately 95% of NPF events were initiated at 8:00-11:00 LT (local time) at the summit of Mt. Tai, which is in good agreement with many previous reports in China (Guo et al., 2012;An et al., 2015;Kulmala et al., 2016;Hao et al., 2015). Since the newly formed particles (about 1 nm) need some time to grow to the measurable diameters, the real start time of NPF would be earlier than the observed time. Previous researches pointed out that this morning time period was associated with enhanced solar radiation, which might correspond to the intensive photochemical activities, leading to potential precursors for NPF (Hallar et al., 2011;Guo et al., 2012). Table 1 lists the calculated parameters of all the NPF events observed at the summit of Mt. Tai, such as formation rate of nucleation mode particles, formation rate of 3 nm particles, growth rate, condensation sink, average sulfuric acid proxy concentration in the early morning (generally corresponding to the time period of 6:00-9:00 LT on Mt. Tai), SO_2 concentration (6:00-13:00 LT), and O_3 concentration (6:00-13:00 LT). Table 2 summarizes the averages, medians, 25th percentiles, 75th percentiles, minima and maxima of these parameters on the basis of Table 1. Table 3 compares the characteristics of NPF on Mt. Tai in the study with those from some other recent studies in China.

The net increase rates and formation rates of nucleation mode particles on Mt. Tai were in the range of 0.96-48.52 cm^{-3} s^{-1} and 1.10-57.43 cm^{-3} s^{-1}, respectively. On average, coagulation loss accounted for 24.6% of the nucleation mode particle formation. The maximum values of the net increase rate, formation rate and SO_2 concentration all occurred on the same day—3 December 2014, and the SO_2 concentration on this day was 12.9±9.6 ppb. The formation rates J_3 varied from 0.82 to 25.04 cm^{-3} s^{-1}, and the median, 25th percentile, and 75th percentile were 6.15, 3.31, and 9.41 cm^{-3} s^{-1}, respectively. On 3 December 2014, J_3 also peaked, showing that NPF event on this day was controlled by sulfuric acid. As shown in Table 3, the particle formation rate at the summit of Mt. Tai was significantly larger than that on the hillside of Mt. Tai Mo Shan

(0.97-10.2 cm^{-3} s^{-1}) and on the top of Mt. Huang (0.09-0.30 cm^{-3} s^{-1}) (Guo et al., 2012;Zhang et al., 2016), but smaller than the results in Beijing and Shanghai (Xiao et al., 2015;Wang et al., 2015). In addition, the observed formation rate on Mt. Tai was slightly larger than the rural and suburban environments included in Table 3 (Liu et al., 2008;Yue et al., 2013;Qi et al., 2015), a fact that was likely associated to intensive precursor transport in the region (eastern China) and enhanced photochemical activity at the summit of Mt. Tai.

Growth rates GR_{3-20} at the summit of Mt. Tai ranged from 0.58 to 7.76 nm h^{-1}, and the median, 25th percentile and 75th percentile were 1.55, 1.15 and 2.51 nm h^{-1}, respectively. Growth rate on Mt. Tai was comparable with some mountain observations such as 1.5-8.4 nm h^{-1} at Mt. Tai Mo Shan, 1.42-4.53 nm h^{-1} on Mt. Huang, and 0.8-3.2 nm h^{-1} on Mt. Daban (Du et al., 2015;Guo et al., 2012;Hao et al., 2015;Zhang et al., 2016). The growth rates observed at the rural, suburban and urban sites were lager than these mountain observations shown in Table 3 (Yue et al., 2013;Liu et al., 2008;Gao et al., 2011;Qi et al., 2015;Xiao et al., 2015), suggesting that relatively clean mountain environment might contain insufficient vapors for newly formed particle growth.

3.2 Condensation sinks and sources of NPF events

Classification of NPF is associated with the persistent high concentration of nucleation mode particles, and occurrence of an NPF event is dependent on the competition between the relevant sinks and sources. Newly formed particles are easily scavenged by the larger pre-existing particles in the atmosphere, leading to their continual reduction in particle number concentration. On the other hand, sufficiently high concentration of low volatility vapors (precursors) could contribute to persistent nucleation, generating new atmospheric particles. Therefore, CS and precursor vapors are the key controlling factors for NPF. Accordingly, as reported by Wang et al. (2011) and Guo et al. (2012), lower CS and higher precursor concentrations are favorable to the NPF events. However, it is difficult to quantify the balance of CS and precursor vapors, and NPF events could be observed in many specific environments. For example, Kulmala et al. (2016) reported that NPF events could be observed in some polluted Chinese megacities with high aerosol loadings. Zhu et al. (2014) showed that NPF occurred in Qingdao City, where a high concentration of gaseous pollutants might offset the effect of large CS. In a semi-rural location in India, Kanawade et al. (2014) demonstrated that NPF events were not limited by lower CS alone. Therefore, a detailed scientific analysis of the sinks and sources in specific atmospheric environments is of great important for NPF.

In this study, CS on NPF days varied from 0.1×10^{-2}-28.4×10^{-2} s^{-1}, corresponding to the median, 25th percentile, and 75th percentile of 0.9×10^{-2} s^{-1}, 0.5×10^{-2} s^{-1} and 1.7×10^{-2} s^{-1}, respectively. This result was much greater than 0.5×10^{-3}-3.5×10^{-3} s^{-1} in Hyytiälä, Finland (Dal Maso et al., 2005), but significantly lower than that at many locations in China such as 0.6×10^{-2}-8.4×10^{-2} s^{-1} in Beijing, 0.9×10^{-2}-3.9×10^{-2} s^{-1} in Nanjing, 0.9×10^{-2}-5.3×10^{-2} in Qingdao, and 1.0×10^{-2}-6.2×10^{-2} s^{-1} in Hong Kong (Zhang et al., 2011;Gao et al., 2012;Guo et al., 2012;An et al., 2015;Herrmann et al., 2014;Zhu et al., 2014).

Overall, the general atmospheric environment at the summit of Mt. Tai is relatively clean in China with low particle loadings.

The hourly average CS on non-NPF days was always higher than that on NPF days, being $(2.0\pm0.5)\times10^{-2}$ s^{-1} and $(1.4\pm0.5)\times10^{-2}$ s^{-1}, respectively. The result indicates that the occurrence of NPF at the summit of Mt. Tai is significantly influenced by the lower CS condition. The general diurnal tendency of CS shows the trough in the morning and the peak in the late afternoon or at night. In the earlier period of a day, the average CS on NPF days was nearly half of the non-NPF days. In the later day, the difference of CS between NPF days and non-NPF days decreased, suggesting that the contribution of NPF on particle concentrations was significant.

Gas-phase sulfuric acid has been identified as an important precursor for the nucleation process. Because direct emission of sulfuric acid is negligible at the summit of Mt. Tai, photochemical reactions of SO_2 would be the significant source for sulfuric acid in the atmosphere, and higher SO_2 concentration can increase the possibility of rich precursors for NPF. In the study, the average SO_2 concentrations between 6:00-13:00 LT on NPF days and non-NPF days were 3.2 ppb and 2.6 ppb, respectively. Figure 1 shows the average diurnal variation of the sulfur dioxide, ozone, temperature, and relative humidity during NPF days and non-NPF days over all the campaigns. Almost all the hourly average SO_2 concentrations on NPF days were higher than the corresponding values on non-NPF days (except for the slightly lower values at 1:00 LT and 3:00 LT) (Fig.1a), suggesting that NPF was really favorable to the high SO_2 concentration.

Figure 2 picked one month's set of continuous data from 10 November to 9 December 2014 for intensive NPF occurrence to visually show the potential correlation between particle number size distribution, gas species, meteorological parameters, $PM_{2.5}$ concentration during NPF events, and the shaded areas represented the NPF days. In Fig. 2, it was noteworthy that the temperature suddenly dropped from 1.3 ℃ to -9.4 ℃ on 30 November 2014. After several days, an exceptionally high SO_2 concentration was observed (7.1 ± 7.2 ppb) at the summit of Mt. Tai (marked in violet block), and frequent NPF events occurred during this period. A possible reason for this observation might be the entrainment of SO_2 from coal or biomass burning in the upwind region when the temperature abruptly changed (Li et al., 2015a;Li et al., 2015b).

Indeed, NPF was not dependent on the high concentration of SO_2 alone, and some of NPF events did not show sensitivity to SO_2 concentration in the study. For example, on 21 September 2014 a non-NPF event occurred with simultaneously high SO_2 concentration (9.7 ± 7.0 ppb during 6:00-13:00 LT) and CS ($4.0\pm1.2\times10^{-2}$ s^{-1} during 6:00-13:00 LT) conditions. Besides, the average $PM_{2.5}$ concentration on this day was as high as 61 μg m^{-3}, much larger than the average of 31 μg m^{-3} at the summit of Mt. Tai. It appeared that the sink dominated the inter-competition between sink and source, which possibly limited the nucleation process. Previous studies have also reported similar phenomena. Song et al. (2010) attributed the weak dependence between SO_2 concentration and NPF events to the intimate coupling between source gases and pre-existing aerosols in South Korea. Therefore, other species accompanying SO_2 emission need to be taken into account for NPF events. Of course, the coupling of SO_2 and the accompanying species at the summit of Mt. Tai may be diluted significantly due to

variable air mass transport.

In this study, a proxy based on SR, SO_2 concentration, CS and RH was used to roughly estimate the magnitudes of sulfuric acid concentration. In the calculations, the average sulfuric acid proxy concentration of all the NPF days was 5.23×10^6 cm^{-3} between 6:00-9:00 LT, which could be comparable with 4.1×10^6 cm^{-3} in Beijing but much lower than 2.3×10^7-6.4×10^7 cm^{-3} in Shanghai and 6.6×10^7-7.8×10^7 cm^{-3} in Nanjing (Wang et al., 2014b;Wang et al., 2015;Xiao et al., 2015). Severely polluted sites generally have the elevated CS, and thus will require a higher concentration of condensable vapors to initiate the nucleation. The fact could be indirectly reflected through many oversea studies in which the NPF events are observed at clean or moderately-polluted sites in the presence of lower sulfuric acid concentrations (Dal Maso et al., 2005;Boy et al., 2005). Apart from other potential precursor species, the lower initial sulfuric acid proxy concentration in the study might be partly explained by the relatively lower CS at the summit of Mt. Tai.

As the most critical nucleation precursor, sulfuric acid is associated with the freshly nucleated particles. Further investigation in the study found that sulfuric acid proxy concentration showed a clear positive correlation with $N_{3\text{-}6}$ on many NPF days, and this positive correlation is consistent with earlier reports (Kulmala et al., 2006;Wang et al., 2011;Guo et al., 2012). As an example, $N_{3\text{-}6}$ reflected a best relationship (R^2 =0.975) with the concentration of sulfuric acid proxy during the NPF event between 6:00 and 14:00 LT on 14 October 2014 (in Fig. 3). After 14:00 LT, the SO_2 concentration increased sharply (a change from 2.6 ppb at 14:00 LT to 19.1 ppb at 15:00), resulting in a lack of correlation between SO_2 concentration and $N_{3\text{-}6}$. In principle, the increase of sulfuric acid concentration should take place earlier than the increase in $N_{3\text{-}6}$. However, there were some NPF days with zero or negative time delay in this study, such as on 14 October 2014 in Fig. 3. Wang et al. (2011) suggested that the pre-formed nucleation mode particles and rapid particle growth might account for such zero or negative time delay.

Wind directions reflect the local situation for air mass, which could indirectly verify the competition between sinks and sources when NPF events occur. Throughout the three campaigns, the dominant wind directions were easterly and westerly, with the main directions being 40 º-110 ºand 220 º-300 º(Fig. 4). Compared with non-NPF days, the wind directions on NPF days had narrower range in the east-southeasterly (85 º-110 º) and west-southwesterly directions (250 º-300 º), as shown in Fig. 4. CS at the summit of Mt. Tai changed with the wind directions, and the average CS in the wind directions between 40 ºand 110 º(2.0×10^{-2} s^{-1}) were almost twice as high as the wind directions between 220 ºand 300 º(1.1×10^{-2} s^{-1}). It is noted that the CS was a relatively small when the wind came from the east-southeast direction, partly explaining the frequent occurrence of NPF events when the wind was from this particular direction. On the other hand, SO_2 concentrations were almost evenly distributed with wind directions in the study, except for the west-southwest direction which corresponded to an elevated SO_2 concentration of 4.3 ppb. For the adjacent wind directions between 220 ºand 350 º, the daily average SO_2 concentrations were only 2.0 ppb. This suggests that potential sources in the west-southwest direction may be contributing to an increase in the probability of NPF occurrence to a certain extent.

O_3 could affect the atmospheric oxidation capacity and photochemical activities, and its oxidation products play a key role in determining the spatial and temporal features of NPF (Guo et al., 2012). For example, O_3 directly reacts with VOCs, or indirectly affect sulfuric acid formation via hydroxyl and hydroperoxy radicals (Berndt et al., 2010;Gómez Martín et al., 2013;Sorribas et al., 2015;Guo et al., 2012). The average O_3 concentrations on NPF days and non-NPF days were 40 ppb and 47 ppb, respectively, and the hourly average O_3 concentrations on NPF days were always lower than those on non-NPF days in Fig. 1b. Previous reports showed that elevated O_3 concentration was beneficial to the occurrence of NPF (An et al., 2015;Guo et al., 2012;Zhang et al., 2016;Huang et al., 2016), but our results did not directly show similar effect. It is known that O_3 is usually contributed by anthropogenic emissions on the ground, such as NO_x and VOCs. Elevated O_3 concentration enhances the atmospheric oxidation capacity, but it may also bring in some other co-linear pollutants simultaneously, such as aged particles. From the aspect of sinks and sources, the sources contributed by O_3 may not always offset the sinks of co-linear pollutants on some non-NPF days with elevated O_3 concentration, leading to the above negative correlation between average O_3 concentration and NPF events. Indeed, there were many NPF events occurred on high level of O_3 conditions, such as the period from 10 November to 17 November 2014 in Fig. 2 (marked in pink block). The positive effect of O_3 on NPF events could not be neglected.

In Fig.1b, the diurnal variation of O_3 concentration at the summit of Mt. Tai had two prominent features - a small trough in the early morning resulting from dry deposition and a broad peak in the afternoon due to formation by solar radiation. As Sun et al. (2016) reported, O_3 concentration between 02:00–05:00 LT could reflect the regional baseline O_3. In the study, the average regional baseline O_3 was 42 ppb, being a relatively high level. The result should be related to the residual O_3 produced in the preceding afternoon in the boundary layer. In addition, the hourly difference values of O_3 between NPF days and non-NPF days in Fig. 1b decreased after 10:00 LT, which was mainly explained by the stronger solar radiation on NPF days.

3.3 Meteorological conditions

Favorable meteorological conditions can promote the occurrence of NPF, especially when the precursors are insufficient in the atmosphere (Song et al., 2010). In this study, approximately 90 % of the NPF events occurred during clear or partial cloudy daytime, suggesting the association between solar radiation and NPF. As discussed earlier, NPF events were initiated at the corresponding time of the solar radiation rapid increase.

The air temperature of all NPF days varied from -11.8 to 22.1 ℃ in this study. The daily temperature profiles were characterized by the expected cosine form of curve, and daily temperature generally oscillated less than 10 ℃ within a day. Temperature at the summit of Mt. Tai exhibited a clear seasonal behavior. As observed in Fig. 1c, the hourly average temperatures on non-NPF days (10.7±1.1 ℃) were always higher than that on NPF days (7.0±1.8 ℃), indicating that NPF events at the summit of Mt. Tai probably favored relatively low temperature. The result is in good agreement with many

previous observations at Mt. Tai Mo Shan (Guo et al., 2012), Mt. Huang (Zhang et al., 2016), and PUY in France (Rose et al., 2015), which all reported the correlation between lower temperature and NPF events. In Guo et al. (2012), it explained that the favorable lower temperature could enhance the bind between sulfuric acid and water molecules. In addition, Young et al. (2007) showed that the effect of lower temperature during NPF events was attributable to atmospheric vertical convection.

The RH on the NPF days ranged from 22% to 95%, and diurnal variation of RH was inversely correlated with the solar radiation. The hourly average RH on NPF days (63±5 %) was always much lower than the corresponding value on non-NPF days (88±2%), and the maximum difference between the two curves in Fig. 1d was about 30%. An anti-correlation between the NPF and RH can be identified at the summit of Mt. Tai, which is in agreement with the results in Beijing, Nanjing, Hong Kong, and Mt. Huang (An et al., 2015;Wang et al., 2014a;Shen et al., 2016;Zhang et al., 2016;Guo et al., 2012). The actual role of RH on NPF is still controversial and has not been resolved. Hamed et al. (2011) indicated that the RH affected the source of NPF via decreasing solar radiation under the high RH conditions. In contrast, simultaneous increasing CS (sink) under the high RH conditions has been suggested as an explanation for the negative effect of the RH (Hamed et al., 2011;Guo et al., 2012).

3.4 Long-range air mass transport

To characterize the influence of the long-range air mass transport on NPF at the summit of Mt. Tai, air mass backward trajectories for 72 h at 6:00 LT at 1535 m ASL were simulated by using the HYSPLIT model developed by the National Oceanic and Atmospheric Administration (NOAA) Air Resources Laboratory. Figure 5a illustrates the air mass backward trajectories of all the NPF days, and Fig. 5b shows for all the non-NPF days.

Based on the transport range and distance, the air mass backward trajectories were classified into three categories in Fig. 5: continental air mass (red), local air mass (green) and maritime air mass (magenta). The majority of transport pathways on NPF days were continental air mass, which accounted for 80% of the total air masses. The continental air mass on NPF days mainly came from the northwest of the observation site, and largely originated from Siberia passing over the long distance across Mongolia, Inner Mongolia, Shanxi Province, Hebei Province, and Beijing. The local and maritime backward trajectories on NPF days accounted for 8% and 12% of the total trajectories, respectively. The local air mass was mainly from surrounding cities such as Jinan, Nanjing, Zhengzhou with the shorter routes, whereas the maritime air mass originated over the Bohai Sea (E-S), Yellow Sea (Y-S) and East China Sea (E-S). The ratios of the continental air mass, local air mass and maritime air mass on non-NPF days were 63%, 12% and 25%, respectively. Overall, the local air mass accounted for the minimum percentage on both NPF and non-NPF days. In addition, comparison between the Fig. 5a and Fig. 5b found that there were much lower percentage of maritime air mass and shorter routes over ocean areas on NPF days. The phenomena were in line with the findings of Peng et al. (2014) who reported without NPF events when the air mass came from the clean ocean side at three coastal sites. Reason for the results was probably that the maritime air mass may not provide enough NPF

precursors to favor the nucleation.

As mentioned above, the continental air mass dominated throughout the observations. According to its transport regions, more polluted continental air mass (Type I) and relatively cleaner continental air mass (Type II) were denoted in the study. Air mass of Type I passed though the heavily polluted areas of Beijing, Hebei Province, Shanxi Province, Henan Province, and Shaanxi Province before reaching the observation site, which could carry a large amount of extra matters. Air mass of Type II was either from the south China or transported over the Bohai Sea (B-S) and Yellow Sea (Y-S), so it represented the relatively clean air masses arriving in Mt. Tai. In this study, four-fifths of the continental air masses on NPF days were Type I, whereas Type I only accounted for two-fifths of the total continental air masses on non-NPF days. These observations seem to suggest that the air masses passing through the heavily polluted areas could increase the occurrence of NPF, Type I air mass probably brought in high levels of precursors for NPF.

In order to further verify the speculation that Type I air mass is in favor of NPF events, Fig. 6 illustrates the average chemical composition of $PM_{2.5}$ and SO_2 concentration in Type I and Type II air masses on NPF days. A prominent increase of average SO_2 concentration was found in Type I, being SO_2 concentration of 3.9 ppb and 1.2 ppb, respectively. The higher SO_2 concentration in Type I air mass suggested that the air masses might pass over the heavily polluted areas and carried the enhanced precursors to Mt. Tai. In addition, the average mass concentrations of $PM_{2.5}$ in Type I and Type II were 33 μg m^{-3} and 23 μg m^{-3}, respectively. The significantly elevated mixing ratios of sulfate, ammonium and nitrate were shown in Type I (in Fig. 6), indicating that transport air masses really passed through polluted S-rich and N-rich areas which might provide potential precursors for NPF.

Long-range air mass transport reflects a regional picture before nucleation, so it should be important for NPF events. The NPF event on 11 November 2014 was picked as a case study to further explore the influence of long-range air mass transport. The time series of the particle size distribution,. trace gases, chemical composition and mass concentration of $PM_{2.5}$ on this day are illustrated in Fig. 7.

In the early morning of 11 November 2014, the average concentrations of SO_2 and $PM_{2.5}$ were 1.7 ppb and 90 μg m^{-3}, respectively. Low SO_2 concentration and extremely high $PM_{2.5}$ concentration made atmospheric nucleation almost impossible. However, an NPF event was observed around noon, and its observed time showed an obvious time delay compared with the general start time of 8:00-11:00 LT in Set. 3.1. In Fig. 7, it found the phenomenon of clear increase in SO_2 concentration, decrease in $PM_{2.5}$ concentration and change in chemical composition of $PM_{2.5}$ simultaneously at about 10:00 LT. Observation site of Mt. Tai is located on the mountain top without any stationary source nearby, and above abrupt changes may suggest that there was another air mass transported to the site, contributing to the NPF event to a certain extent. During 6:00-9:00 LT, the average mass concentrations of sulfate, ammonium, nitrate, OC and EC in $PM_{2.5}$ were 4.1, 4.6, 4.1, 7.6 and 0.7 μg m^{-3}, respectively. In contrast, their average concentrations changed as 13.1, 11.2, 11.1, 10.0 and 0.2 μg m^{-3} during 11:00-18:00 LT. The mixing ratio of sulfate in $PM_{2.5}$ increased significantly before and after 10:00 LT, suggesting

that the new transport air mass might be S (SO_2)-rich.

In order to verify above results, air mass backward trajectories for 72 h at 1535 m ASL at 14:00, 12:00, 10:00, 8:00 and 6:00 LT on 11 November 2014 are shown in Fig. 8. It illustrates that the origin of the transport air mass moved from eastern China (Jiangsu and Anhui Provinces, lines A and B) to western China (lines C, D and E) at about 10:00 LT, which was in agreement with the earlier analysis in Fig. 7. The latter air mass backward trajectories (line C, D and E) passed through the heavily polluted areas, such as Shanxi and Shaanxi Provinces, before reaching the site of Mt. Tai, leading to the potential increase of precursor concentrations.

4. Conclusions

Field observations of NPF at the mountain-top sites are scarce in China, and the results of such studies could significantly contribute to atmospheric aerosol pollution control. A comprehensive investigation of NPF was conducted at the summit of Mt. Tai (1534 m ASL), eastern China, from 25 July to 24 August 2014 (Phase I), 21 September to 9 December 2014 (Phase II) and 16 June to 7 August 2015 (Phase III), using two types of size distribution instruments (NAIS and WPS) and including two trace gases, multiple meteorological parameters, and mass concentration and chemical composition of $PM_{2.5}$.

During the 164 days, 66 NPF events were identified based on the particle size distribution, giving an occurrence frequency of 40% overall. The J_3, $J_{3\text{-}20}$, and growth rates were in the range of 0.82-25.04 cm^{-3} s^{-1}, 1.10-57.43 cm^{-3} s^{-1}, and 0.58-7.76 nm h^{-1}, respectively. In comparison with other studies in China, particle formation rate at the summit of Mt. Tai was slightly greater than those in some rural and suburban environments, which probably was associated with the intensive air mass transport in eastern China and enhanced solar radiation at the summit of Mt. Tai. Instead, growth rate was lower in this study than in some rural, suburban and urban environments of China, suggesting insufficient precursors for particle growth on Mt. Tai.

On average, the condensation sink (CS), O_3 concentration, air temperature and relative humidity were lower, whereas the SO_2 concentration was higher on NPF days than on non-NPF days. Occurrence of an NPF event is mainly dependent on the competition between the sinks and sources, and factors such as trace gases, meteorological conditions, air mass transport are all through affecting sinks and sources in determining the NPF.

Air mass backward trajectories in the study were classified into three categories of continental, local and maritime air masses, among which continental air mass was the majority. The continental air masses passing through more polluted areas (denoted as Type I) may contribute to an increased the frequency of NPF events, which can be explained by the high level of precursors carried from the polluted regions. In addition, maritime air mass may not favorable condition for NPF because of potential lack of precursors.

Acknowledgements. This work was supported by National Natural Science Foundation of China (No. 41375126), Mount Tai Scholar Grand (ts20120552), Cyrus Tang Foundation (No.CTF-FD2014001), Ministry of Science and Technology of China (SQ2016ZY01002231, 2014BAC22B01), and Marie Skłodowska-Curie Actions (H2020-MSCA-RISE-2015-690958).

References

Allan, J. D., Williams, P. I., Najera, J., Whitehead, J. D., Flynn, M. J., Taylor, J. W., Liu, D., Darbyshire, E., Carpenter, L. J., Chance, R., Andrews, S. J., Hackenberg, S. C., and McFiggans, G.: Iodine observed in new particle formation events in the Arctic atmosphere during ACCACIA, Atmos. Chem. Phys., 15, 5599-5609, 10.5194/acp-15-5599-2015, 2015.

An, J., Wang, H., Shen, L., Zhu, B., Zou, J., Gao, J., and Kang, H.: Characteristics of new particle formation events in Nanjing, China: Effect of water-soluble ions, Atmos. Environ., 108, 32-40, 10.1016/j.atmosenv.2015.01.038, 2015.

Berndt, T., Stratmann, F., Sipilä, M., Vanhanen, J., Petäjä, T., Mikkilä, J., Grüner, A., Spindler, G., Lee Mauldin Iii, R., Curtius, J., Kulmala, M., and Heintzenberg, J.: Laboratory study on new particle formation from the reaction OH + SO_2 : influence of experimental conditions, H_2O vapour, NH_3 and the amine tert-butylamine on the overall process, Atmos. Chem. Phys., 10, 7101-7116, 10.5194/acp-10-7101-2010, 2010.

Boy, M., Kulmala, M., Ruuskanen, T. M., Pihlatie, M., Reissell, A., Aalto, P. P., Keronen, P., Dal Maso, M., Hellen, H., Hakola, H., Jansson, R., Hanke, M., and Arnold, F.: Sulphuric acid closure and contribution to nucleation mode particle growth, Atmos. Chem. Phys., 5, 863-878, 10.5194/acp-5-863-2005, 2005.

Butt, E. W., Rap, A., Schmidt, A., Scott, C. E., Pringle, K. J., Reddington, C. L., Richards, N. A. D., Woodhouse, M. T., Ramirez-Villegas, J., Yang, H., Vakkari, V., Stone, E. A., Rupakheti, M., S. Praveen, P., G. van Zyl, P., P. Beukes, J., Josipovic, M., Mitchell, E. J. S., Sallu, S. M., Forster, P. M., and Spracklen, D. V.: The impact of residential combustion emissions on atmospheric aerosol, human health, and climate, Atmos. Chem. Phys., 16, 873-905, 10.5194/acp-16-873-2016, 2016.

Chiharu, N., Kazuo, O., Mizuka, K., Katsuji, M., and Yasunobu, I.: Nucleation mode particles in upslope valley winds at Mount Norikura, Japan: Implications for the vertical extent of new particle formation events in the lower troposphere, J. Geophys. Res., 113, 10.1029/2007jd009302, 2008.

Dal Maso, M., Kulmala, M., Lehtinen, K. E. J., Mäkelä, J. M., Aalto, P., and O'Dowd, D.: Condensation and coagulation sinks and formation of nucleation mode particles in coastal and boreal forest boundary layers, J. Geophys. Res., 107, 8097, 10.1029/2001JD001053, 2002.

Dal Maso, M., Kulmala, M., Riipinen, I., Wagner, R., Hussein, T., Aalto, P. P., and Lehtinen, K. E. J.: Formation and growth of fresh atmospheric aerosols : Eight Years of Aerosol Size Distribution Data from SMEAR II, Hyytiälä, Finland, Boreal Environ. Res., 10, 323-336, 2005.

Du, W., Sun, Y. L., Xu, Y. S., Jiang, Q., Wang, Q. Q., Yang, W., Wang, F., Bai, Z. P., Zhao, X. D., and Yang, Y. C.: Chemical characterization of submicron aerosol and particle growth events at a national background site (3295 m a.s.l.) in the Tibetan Plateau, Atmos. Chem. Phys., 15, 10811-10824, 10.5194/acp-15-10811-2015, 2015.

Gómez Martín, J. C., Gálvez, O., Baeza-Romero, M. T., Ingham, T., Plane, J. M., and Blitz, M. A.: On the mechanism of iodine oxide particle formation, Phys. Chem. Chem. Phys., 15, 15612-15622, 10.1039/c3cp51217g, 2013.

Gao, J., Wang, T., Zhou, X., Wu, W., and Wang, W.: Measurement of aerosol number size distributions in the Yangtze River delta in China: Formation and growth of particles under polluted conditions, Atmos. Environ., 43, 829-836, 10.1016/j.atmosenv.2008.10.046, 2009.

Gao, J., Chai, F., Wang, T., and Wang, W.: Particle number size distribution and new particle formation (NPF) in Lanzhou, Western China, Particuology, 9, 611-618, 10.1016/j.partic.2011.06.008, 2011.

Gao, J., Chai, F., Wang, T., Wang, S., and Wang, W.: Particle number size distribution and new particle formation: New characteristics during the special pollution control period in Beijing, J. Environ. Sci., 24, 14-21, 10.1016/s1001-0742(11)60725-0, 2012.

Gong, Y., Hu, M., Cheng, Y., Su, H., Yue, D., Liu, F., Wiedensohler, A., Wang, Z., Kalesse, H., and Liu, S.: Competition of coagulation sink and source rate: New particle formation in the Pearl River Delta of China, Atmos. Environ., 44, 3278-3285, 10.1016/j.atmosenv.2010.05.049, 2010.

Guo, H., Wang, D. W., Cheung, K., Ling, Z. H., Chan, C. K., and Yao, X. H.: Observation of aerosol size distribution and new particle formation at a mountain site in subtropical Hong Kong, Atmos. Chem. Phys., 12, 9923-9939, 10.5194/acp-12-9923-2012, 2012.

Guo, S., Hu, M., Zamora, M. L., Peng, J., Shang, D., Zheng, J., Du, Z., Wu, Z., Shao, M., Zeng, L., Molina, M. J., and Zhang, R.: Elucidating severe urban haze formation in China, Proc. Natl. Acad. Sci. U S A, 111, 17373-17378, 10.1073/pnas.1419604111, 2014.

Hallar, A. G., Lowenthal, D. H., Chirokova, G., Borys, R. D., and Wiedinmyer, C.: Persistent daily new particle formation at a mountain-top location, Atmos. Environ., 45, 4111-4115, 10.1016/j.atmosenv.2011.04.044, 2011.

Hamed, A., Korhonen, H., Sihto, S.-L., Joutsensaari, J., Järvinen, H., Petäjä, T., Arnold, F., Nieminen, T., Kulmala, M., Smith, J. N., Lehtinen, K. E. J., and Laaksonen, A.: The role of relative humidity in continental new particle formation, J. Geophys. Res., 116, 909-926, 10.1029/2010jd014186, 2011.

Han, S.: Effect of Aerosols on Visibility and Radiation in Spring 2009 in Tianjin, China, Aerosol Air Qual. Res., 12, 211-217, 10.4209/aaqr.2011.05.0073, 2012.

Hao, J., Yin, Y., Li, X., Yuan, L., and Xiao, H.: Observations of Nucleation Mode Particles Formation and Growth on Mount Huang, China, Procedia Engineering, 102, 1167-1176, 10.1016/j.proeng.2015.01.242, 2015.

Herrmann, E., Ding, A. J., Kerminen, V. M., Petäjä, T., Yang, X. Q., Sun, J. N., Qi, X. M., Manninen, H., Hakala, J.,

Nieminen, T., Aalto, P. P., Kulmala, M., and Fu, C. B.: Aerosols and nucleation in eastern China: first insights from the new SORPES-NJU station, Atmos. Chem. Phys., 14, 2169-2183, 10.5194/acp-14-2169-2014, 2014.

Hu, M., Shang, D., Guo, S., and Wu, Z.: Mechanism of New Particle Formation and Growth as well as Environmental Effects under Complex Air Pollution in China, Acta Chimica Sinica, 74, 385-391, 10.6023/a16020105, 2016.

Huang, X., Zhou, L., Ding, A., Qi, X., Nie, W., Wang, M., Chi, X., Petäjä, T., Kerminen, V.-M., Roldin, P., Rusanen, A., Kulmala, M., and Boy, M.: Comprehensive modelling study on observed new particle formation at the SORPES station in Nanjing, China, Atmos. Chem. Phys., 16, 2477-2492, 10.5194/acp-16-2477-2016, 2016.

Kanawade, V. P., Shika, S., Pöhlker, C., Rose, D., Suman, M. N. S., Gadhavi, H., Kumar, A., Nagendra, S. M. S., Ravikrishna, R., Yu, H., Sahu, L. K., Jayaraman, A., Andreae, M. O., Pöschl, U., and Gunthe, S. S.: Infrequent occurrence of new particle formation at a semi-rural location, Gadanki, in tropical Southern India, Atmos. Environ., 94, 264-273, 10.1016/j.atmosenv.2014.05.046, 2014.

Kazil, J., Stier, P., Zhang, K., Quaas, J., Kinne, S., O'Donnell, D., Rast, S., Esch, M., Ferrachat, S., Lohmann, U., and Feichter, J.: Aerosol nucleation and its role for clouds and Earth's radiative forcing in the aerosol-climate model ECHAM5-HAM, Atmos. Chem. Phys., 10, 10733-10752, 10.5194/acp-10-10733-2010, 2010.

Kuang, C., Riipinen, I., Sihto, S. L., Kulmala, M., McCormick, A. V., and McMurry, P. H.: An improved criterion for new particle formation in diverse atmospheric environments, Atmos. Chem. Phys., 10, 8469-8480, 10.5194/acp-10-8469-2010, 2010.

Kulmala, M., Dal Maso, M., Mäkelä, M., Pirjola, L., Väkevä, M., Aalto, P., Miikkulainen, P., and Hämeri, K.: On the formation, growth and composition of nucleation mode particles, Tellus B, 53, 479-490, 10.1034/j.1600-0889.2001.d01-33.x, 2001.

Kulmala, M., Vehkamäki, H., Petäjä, T., Dal Maso, M., Lauri, A., Kerminen, V. M., Birmili, W., and McMurry, P. H.: Formation and growth rates of ultrafine atmospheric particles: a review of observations, J. Aerosol Sci., 35, 143-176, 10.1016/j.jaerosci.2003.10.003, 2004.

Kulmala, M., Lehtinen, K. E. J., and Laaksonen, A.: Cluster activation theory as an explanation of the linear dependence between formation rate of 3 nm particles and sulphuric acid concentration, Atmos. Chem. Phys., 6, 787-793, 10.5194/acp-6-787-2006, 2006.

Kulmala, M., Petäjä, T., Nieminen, T., Sipila, M., Manninen, H. E., Lehtipalo, K., Dal Maso, M., Aalto, P. P., Junninen, H., Paasonen, P., Riipinen, I., Lehtinen, K. E., Laaksonen, A., and Kerminen, V. M.: Measurement of the nucleation of atmospheric aerosol particles, Nat. Protoc., 7, 1651-1667, 10.1038/nprot.2012.091, 2012.

Kulmala, M., Petäjä, T., Kerminen, V. M., Kujansuu, J., Ruuskanen, T., Ding, A. J., Nie, W., Hu, M., Wang, Z. B., Wu, Z. J., Wang, L., and Worsnop, D. R.: On secondary new particle formation in China, Front. Environ. Sci. Eng., 10, 08, 10.1007/s11783-016-0850-1, 2016.

Li, T., Wang, Y., Li, W. J., Chen, J. M., Wang, T., and Wang, W. X.: Concentrations and solubility of trace elements in fine particles at a mountain site, southern China: regional sources and cloud processing, Atmos. Chem. Phys., 15, 8987-9002, 10.5194/acp-15-8987-2015, 2015a.

Li, W. J., Zhang, D. Z., Shao, L. Y., Zhou, S. Z., and Wang, W. X.: Individual particle analysis of aerosols collected under haze and non-haze conditions at a high-elevation mountain site in the North China plain, Atmos. Chem. Phys., 11, 11733-11744, 10.5194/acp-11-11733-2011, 2011.

Li, W. J., Chen, S. R., Xu, Y. S., Guo, X. C., Sun, Y. L., Yang, X. Y., Wang, Z. F., Zhao, X. D., Chen, J. M., and Wang, W. X.: Mixing state and sources of submicron regional background aerosols in the northern Qinghai–Tibet Plateau and the influence of biomass burning, Atmos. Chem. Phys., 15, 13365-13376, 10.5194/acp-15-13365-2015, 2015b.

Liu, S., Hu, M., Wu, Z., Wehner, B., Wiedensohler, A., and Cheng, Y.: Aerosol number size distribution and new particle formation at a rural/coastal site in Pearl River Delta (PRD) of China, Atmos. Environ., 42, 6275-6283, 10.1016/j.atmosenv.2008.01.063, 2008.

Liu, X. H., Zhu, Y. J., Zheng, M., Gao, H. W., and Yao, X. H.: Production and growth of new particles during two cruise campaigns in the marginal seas of China, Atmos. Chem. Phys., 14, 7941-7951, 10.5194/acp-14-7941-2014, 2014.

Manninen, H. E., Nieminen, T., Asmi, E., Gagné, S., Häkkinen, S., Lehtipalo, K., Aalto, P., Vana, M., Mirme, A., Mirme, S., Hõrrak, U., Plass-Dülmer, C., Stange, G., Kiss, G., Hoffer, A., Törő, N., Moerman, M., Henzing, B., de Leeuw, G., Brinkenberg, M., Kouvarakis, G. N., Bougiatioti, A., Mihalopoulos, N., O'Dowd, C., Ceburnis, D., Arneth, A., Svenningsson, B., Swietlicki, E., Tarozzi, L., Decesari, S., Facchini, M. C., Birmili, W., Sonntag, A., Wiedensohler, A., Boulon, J., Sellegri, K., Laj, P., Gysel, M., Bukowiecki, N., Weingartner, E., Wehrle, G., Laaksonen, A., Hamed, A., Joutsensaari, J., Petäjä, T., Kerminen, V. M., and Kulmala, M.: EUCAARI ion spectrometer measurements at 12 European sites-analysis of new particle formation events, Atmos. Chem. Phys., 10, 7907-7927, 10.5194/acp-10-7907-2010, 2010.

Mikkonen, S., Romakkaniemi, S., Smith, J. N., Korhonen, H., Petäjä, T., Plass-Duelmer, C., Boy, M., McMurry, P. H., Lehtinen, K. E. J., Joutsensaari, J., Hamed, A., Mauldin Iii, R. L., Birmili, W., Spindler, G., Arnold, F., Kulmala, M., and Laaksonen, A.: A statistical proxy for sulphuric acid concentration, Atmos. Chem. Phys., 11, 11319-11334, 10.5194/acp-11-11319-2011, 2011.

Nie, W., Ding, A., Wang, T., Kerminen, V. M., George, C., Xue, L., Wang, W., Zhang, Q., Petaja, T., Qi, X., Gao, X., Wang, X., Yang, X., Fu, C., and Kulmala, M.: Polluted dust promotes new particle formation and growth, Sci. Rep., 4, 6634, 10.1038/srep06634, 2014.

Peng, J. F., Hu, M., Wang, Z. B., Huang, X. F., Kumar, P., Wu, Z. J., Guo, S., Yue, D. L., Shang, D. J., Zheng, Z., and He, L. Y.: Submicron aerosols at thirteen diversified sites in China: size distribution, new particle formation and corresponding contribution to cloud condensation nuclei production, Atmos. Chem. Phys., 14, 10249-10265, 10.5194/acp-14-10249-2014, 2014.

Qi, X. M., Ding, A. J., Nie, W., Petäjä, T., Kerminen, V. M., Herrmann, E., Xie, Y. N., Zheng, L. F., Manninen, H., Aalto, P., Sun, J. N., Xu, Z. N., Chi, X. G., Huang, X., Boy, M., Virkkula, A., Yang, X. Q., Fu, C. B., and Kulmala, M.: Aerosol size distribution and new particle formation in western Yangtze River Delta of China: two-year measurement at the SORPES station, Atmos. Chem. Phys., 15, 12491-12537, 10.5194/acpd-15-12491-2015, 2015.

Rose, C., Sellegri, K., Asmi, E., Hervo, M., Freney, E., Colomb, A., Junninen, H., Duplissy, J., Sipilä, M., Kontkanen, J., Lehtipalo, K., and Kulmala, M.: Major contribution of neutral clusters to new particle formation at the interface between the boundary layer and the free troposphere, Atmos. Chem. Phys., 15, 3413-3428, 10.5194/acp-15-3413-2015, 2015.

Saunders, R. W., Kumar, R., Martin, J. C. G., Mahajan, A. S., Murray, B. J., and Plane, J. M. C.: Studies of the Formation and Growth of Aerosol from Molecular Iodine Precursor, Z. Phys. chem., 224, 1095-1117, 10.1524/zpch.2010.6143, 2010.

Shen, X. J., Sun, J. Y., Zhang, X. Y., Zhang, Y. M., Zhang, L., Fan, R. X., Zhang, Z. X., Zhang, X. L., Zhou, H. G., Zhou, L. Y., Dong, F., and Shi, Q. F.: The influence of emission control on particle number size distribution and new particle formation during China's V-Day parade in 2015, Sci. Total Environ., 573, 409-419, 10.1016/j.scitotenv.2016.08.085, 2016.

Sihto, S.-L., Kulmala, M., Kerminen, V.-M., Dal Maso, M., Petäjä, T., Riipinen, I., Korhonen, H., Arnold, F., Janson, R., Boy, M., Laaksonen, A., and Lehtinen, K. E. J.: Atmospheric sulphuric acid and aerosol formation implications from atmospheric measurements for nucleation and early growth mechanisms, Atmos. Chem. Phys., 6, 4079-4091, 10.5194/acp-6-4079-2006, 2006.

Song, M., Lee, M., Kim, J. H., Yum, S. S., Lee, G., and Kim, K.-R.: New particle formation and growth in relation to vertical mixing and chemical species during ABC-EAREX2005, Atmos. Res., 97, 359-370, 10.1016/j.atmosres.2010.04.013, 2010.

Sorribas, M., Adame, J. A., Olmo, F. J., Vilaplana, J. M., Gil-Ojeda, M., and Alados-Arboledas, L.: A long-term study of new particle formation in a coastal environment: meteorology, gas phase and solar radiation implications, Sci. Total Environ., 511, 723-737, 10.1016/j.scitotenv.2014.12.011, 2015.

Spracklen, D. V., Carslaw, K. S., Kulmala, M., Kerminen, V.-M., Sihto, S.-L., Riipinen, I., Merikanto, J., Mann, G. W., Chipperfield, M. P., Wiedensohler, A., Birmili, W., and Lihavainen, H.: Contribution of particle formation to global cloud condensation nuclei concentrations, Geophys. Res. Lett., 35, 160-162, 10.1029/2007gl033038, 2008.

Sun, L., Xue, L. K., Wang, T., Gao, J., Ding, A. J., Cooper, O. R., Lin, M. Y., Xu, P. J., Wang, Z., Wang, X. F., Wen, L., Zhu, Y. H., Chen, T. S., Yang, L. X., Wang, Y., Chen, J. M., and Wang, W. X.: Significant increase of summertime ozone at Mount Tai in Central Eastern China, Atmos. Chem. Phys., 16, 10637-10650, 10.5194/acp-16-10637-2016, 2016.

Venzac, H., Sellegri, K., Laj, P., Villani, P., Bonasoni, P., Marinoni, A., Cristofanelli, P., Calzolari, F., Fuzzi, S., Decesari, S., Facchini, M. C., Vuillermoz, E., and Verza, G. P.: High frequency new particle formation in the Himalayas, Proc. Natl. Acad. Sci. USA, 105, 15666-15671, 10.1073/pnas.0801355105, 2008.

Wang, D. W., Guo, H., Cheung, K., and Gan, F. X.: Observation of nucleation mode particle burst and new particle formation events at an urban site in Hong Kong, Atmos. Environ., 99, 196-205, 10.1016/j.atmosenv.2014.09.074, 2014a.

Wang, H., Zhu, B., Shen, L., An, J., Yin, Y., and Kang, H.: Number size distribution of aerosols at Mt. Huang and Nanjing in the Yangtze River Delta, China: Effects of air masses and characteristics of new particle formation, Atmos. Res., 150, 42-56, 10.1016/j.atmosres.2014.07.020, 2014b.

Wang, Z. B., Hu, M., Yue, D. L., Zheng, J., Zhang, R. Y., Wiedensohler, A., Wu, Z. J., Nieminen, T., and Boy, M.: Evaluation on the role of sulfuric acid in the mechanisms of new particle formation for Beijing case, Atmos. Chem. Phys., 11, 12663-12671, 10.5194/acp-11-12663-2011, 2011.

Wang, Z. B., Hu, M., Wu, Z. J., and Yue, D. L.: Reasearch on the Formation Mechanisms of New Particles in the Atmosphere, Acta. Chim. Sinica, 71, 519-527, 10.6023/a12121062, 2013.

Wang, Z. B., Hu, M., Pei, X. Y., Zhang, R. Y., Paasonen, P., Zheng, J., Yue, D. L., Wu, Z. J., Boy, M., and Wiedensohler, A.: Connection of organics to atmospheric new particle formation and growth at an urban site of Beijing, Atmos. Environ., 103, 7-17, 10.1016/j.atmosenv.2014.11.069, 2015.

Wehner, B., Wiedensohler, A., Tuch, T. M., Wu, Z. J., Hu, M., Slanina, J., and Kiang, C. S.: Variability of the aerosol number size distribution in Beijing, China: New particle formation, dust storms, and high continental background, Geophys. Res. Lett., 31, L22108, 10.1029/2004gl021596, 2004.

Weingartner, E., Nyeki, S., and Baltensperger, U.: Seasonal and diurnal variation of aerosol size distributions (10<D<750 nm) at a high-alpine site (Jungfraujoch 3580 m asl), J. Geophys. Res., 104, 26809-26820, 10.1029/1999jd900170, 1999.

Xiao, S., Wang, M. Y., Yao, L., Kulmala, M., Zhou, B., Yang, X., Chen, J. M., Wang, D. F., Fu, Q. Y., Worsnop, D. R., and Wang, L.: Strong atmospheric new particle formation in winter in urban Shanghai, China, Atmos. Chem. Phys., 15, 1769-1781, 10.5194/acp-15-1769-2015, 2015.

Young, L. H., Benson, D. R., Montanaro, W. M., Lee, S. H., Pan, L. L., Rogers, D. C., Jensen, J., Stith, J. L., Davis, C. A., Campos, T. L., Bowman, K. P., Cooper, W. A., and Lait, L. R.: Enhanced new particle formation observed in the northern midlatitude tropopause region, J. Geophys. Res.- Atmos., 112, D10218, 10.1029/2006JD008109, 2007.

Yue, D. L., Hu, M., Wang, Z. B., Wen, M. T., Guo, S., Zhong, L. J., Wiedensohler, A., and Zhang, Y. H.: Comparison of particle number size distributions and new particle formation between the urban and rural sites in the PRD region, China, Atmos. Environ., 76, 181-188, 10.1016/j.atmosenv.2012.11.018, 2013.

Zhang, R.: Getting to the Critical Nucleus of Aerosol Formation, Science, 328, 1366-1367, 2010.

Zhang, R., Khalizov, A., Wang, L., Hu, M., and Xu, W.: Nucleation and growth of nanoparticles in the atmosphere, Chem. Rev., 112, 1957-2011, 10.1021/cr2001756, 2012.

Zhang, X., Yin, Y., Lin, Z., Han, Y., Hao, J., Yuan, L., Chen, K., Chen, J., Kong, S., Shan, Y., Xiao, H., and Tan, W.: Observation of aerosol number size distribution and new particle formation at a mountainous site in Southeast China, Sci. Total Environ., 575, 309-320, 10.1016/j.scitotenv.2016.09.212, 2016.

Zhang, X. H., Zhang, Y. M., Sun, J. Y., Zheng, X. J., Li, G., and Deng, Z. Q.: Characterization of particle number size

distribution and new particle formation in an urban environment in Lanzhou, China, J. Aerosol Sci., 103, 53-66, 10.1016/j.jaerosci.2016.10.010, 2017.

Zhang, Y. M., Zhang, X. Y., Sun, J. Y., Lin, W. L., Gong, S. L., Shen, X. J., and Yang, S.: Characterization of new particle and secondary aerosol formation during summertime in Beijing, China, Tellus B, 63, 382-394, 10.1111/j.1600-0889.2011.00533.x, 2011.

Zhang, Y. M., Zhang, X. Y., Sun, J. Y., Hu, G. Y., Shen, X. J., Wang, Y. Q., Wang, T. T., Wang, D. Z., and Zhao, Y.: Chemical composition and mass size distribution of PM1 at an elevated site in central east China, Atmos. Chem. Phys., 14, 12237-12249, 10.5194/acp-14-12237-2014, 2014.

Zhu, Y., Sabaliauskas, K., Liu, X., Meng, H., Gao, H., Jeong, C.-H., Evans, G. J., and Yao, X.: Comparative analysis of new particle formation events in less and severely polluted urban atmosphere, Atmos. Environ., 98, 655-664, 10.1016/j.atmosenv.2014.09.043, 2014.

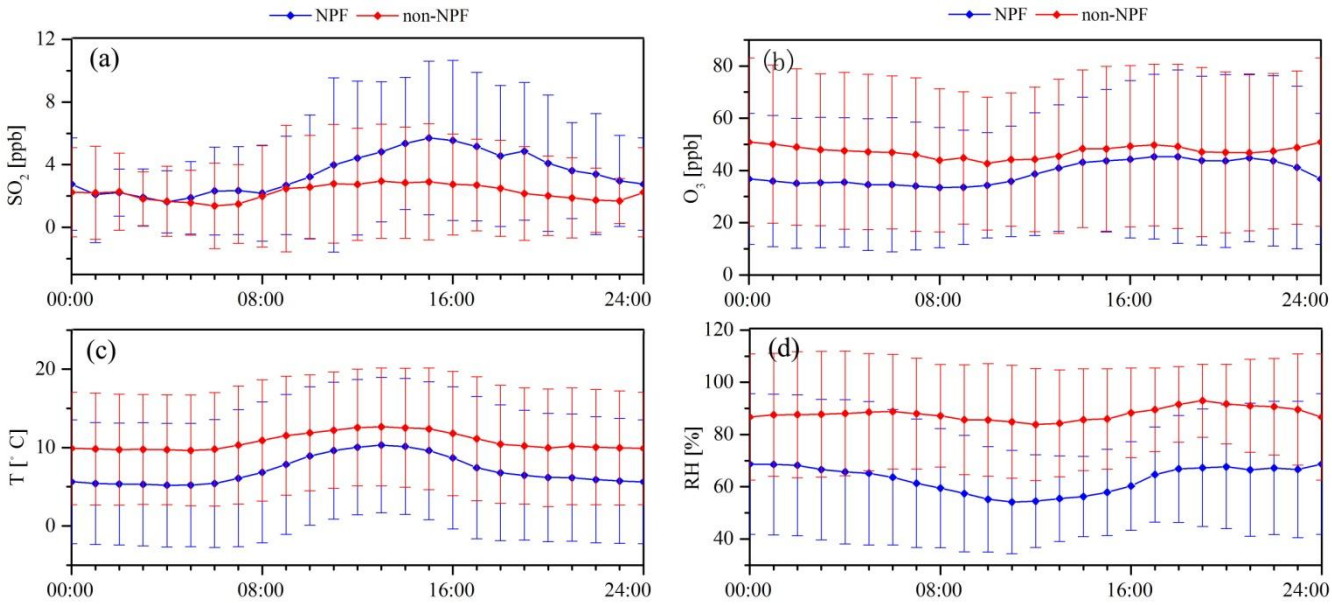

Fig. 1. Average diurnal variations of trace gases (SO_2 and O_3) and meteorological conditions (T and RH) during NPF days and non-NPF days over all the campaigns at the summit of Mt. Tai

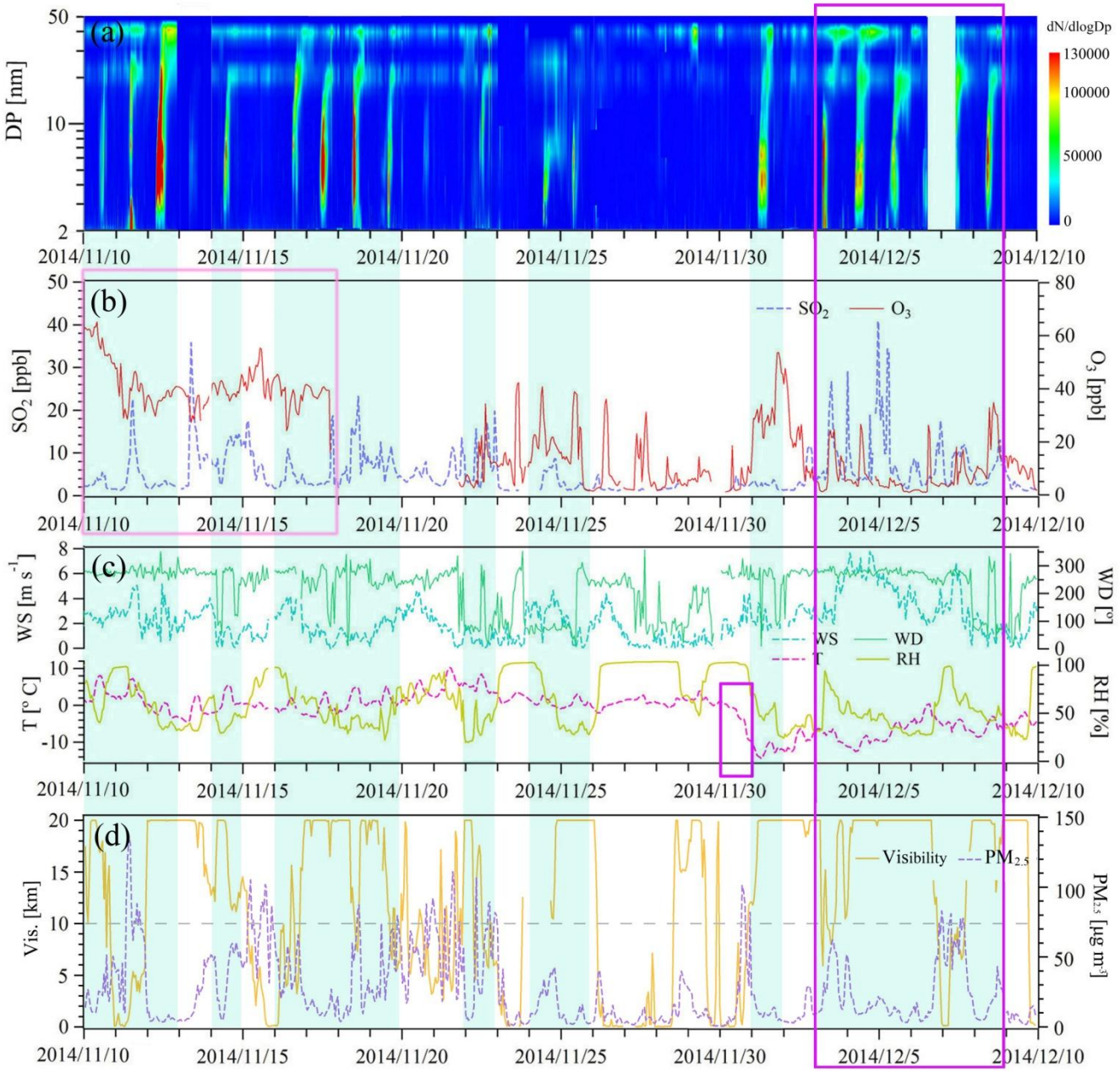

Fig. 2. Time series during 10 November-9 December 2014, and the shaded areas represent the NPF days: (a) contour plot of particle number size distribution using NAIS data; (b) sulfur dioxide (blue) and ozone (red); (c) meteorological parameters, including wind speed (cyan), wind direction (green), temperature (magenta) and relative humidity (earth yellow); (d) visibility (yellow) and $PM_{2.5}$ concentration (purple), and the gray line is the boundary for 10 km and 75 μg m^{-3}.

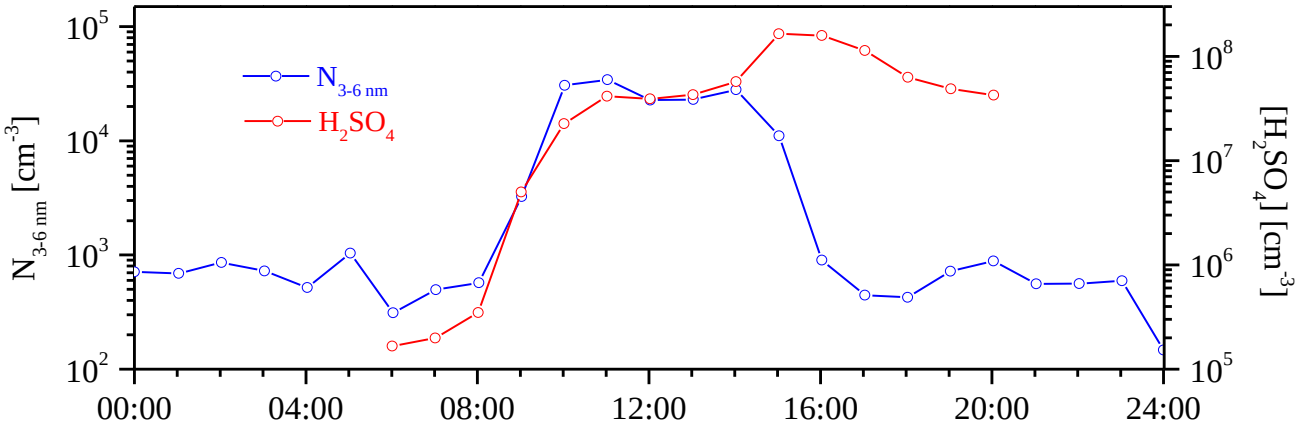

Fig. 3. The particle number concentration of 3-6 nm ($N_{3\text{-}6}$, blue) and sulfuric acid proxy concentration ([H_2SO_4], red) on 14 October 2014, fitting a good relationship (R^2 =0.975) between 6:00-14:00 LT during the NPF event.

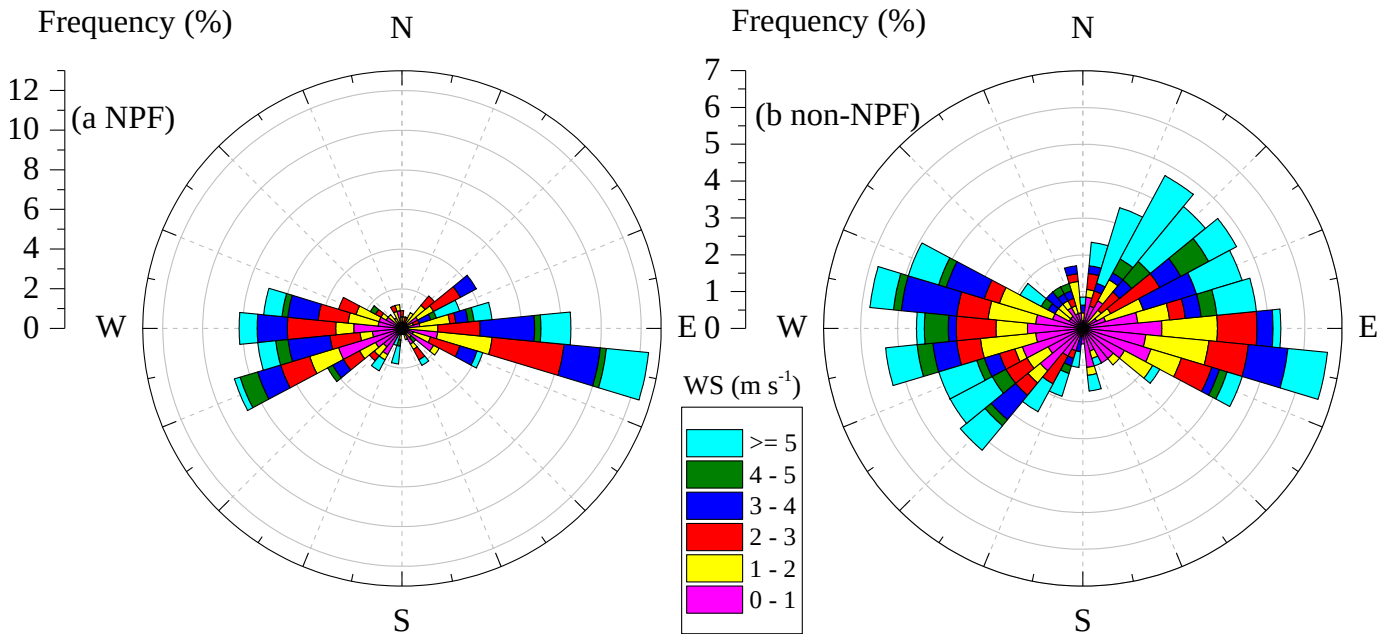

Fig. 4. Wind rose plots of all the NPF days (a) and non-NPF days (b), and the wind speed and wind direction between 06:00 and 11:00 LT are included. Length of each spoke on the circle represents the probability of wind coming from a particular direction at the certain range of wind speed.

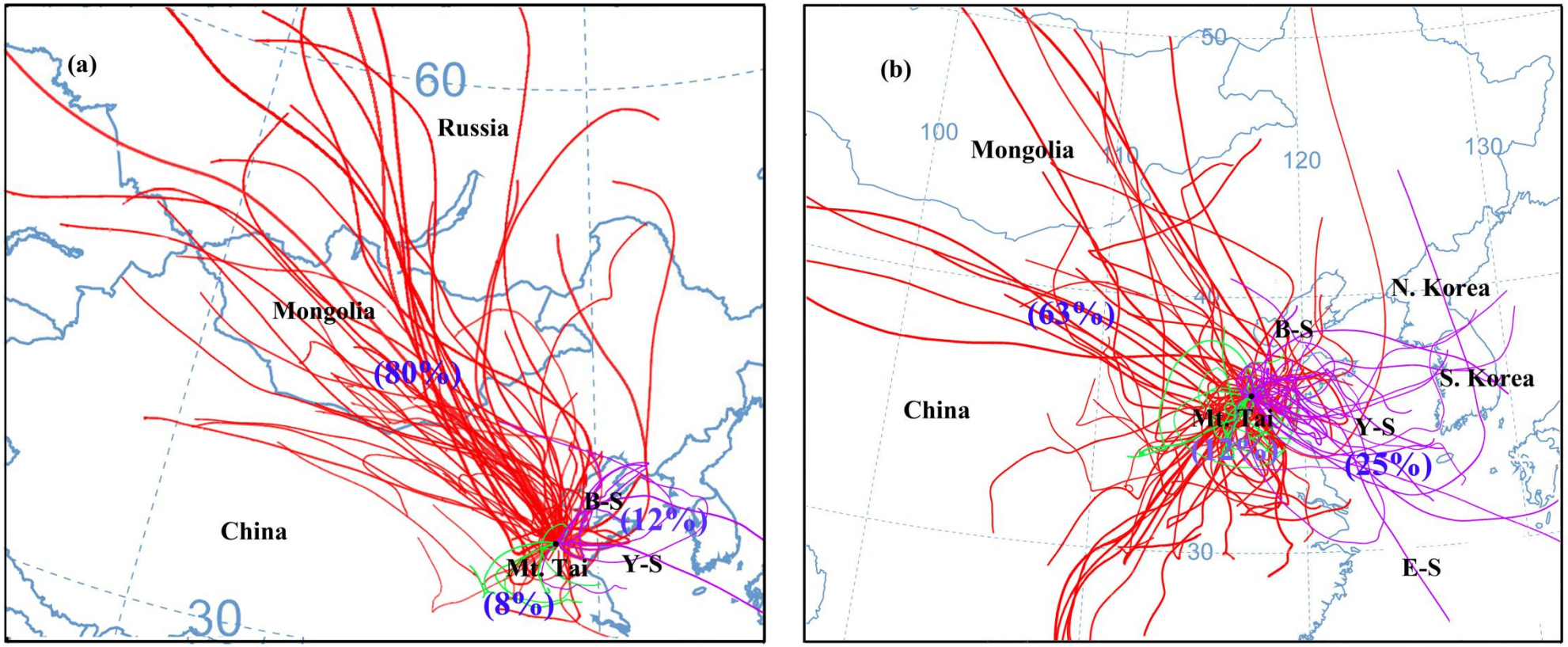

Fig. 5. Air mass back trajectories for 72 h at 6:00 LT at 1535 m ASL on all the NPF days (a) and non-NPF days (b), and the continental air mass, local air mass and maritime air mass are represented in red, green and magenta, respectively.

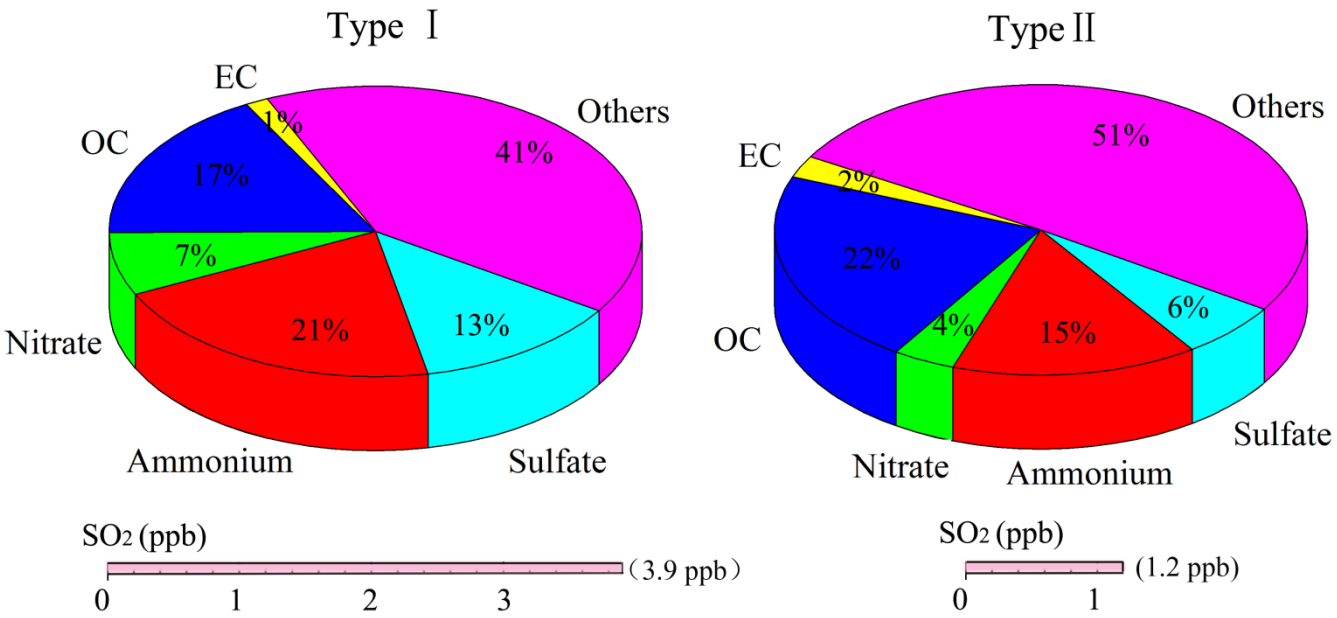

Fig. 6. The average chemical composition of $PM_{2.5}$ and SO_2 concentration in more polluted continental air mass (Type I) and relatively cleaner continental air mass (Type II) on NPF days

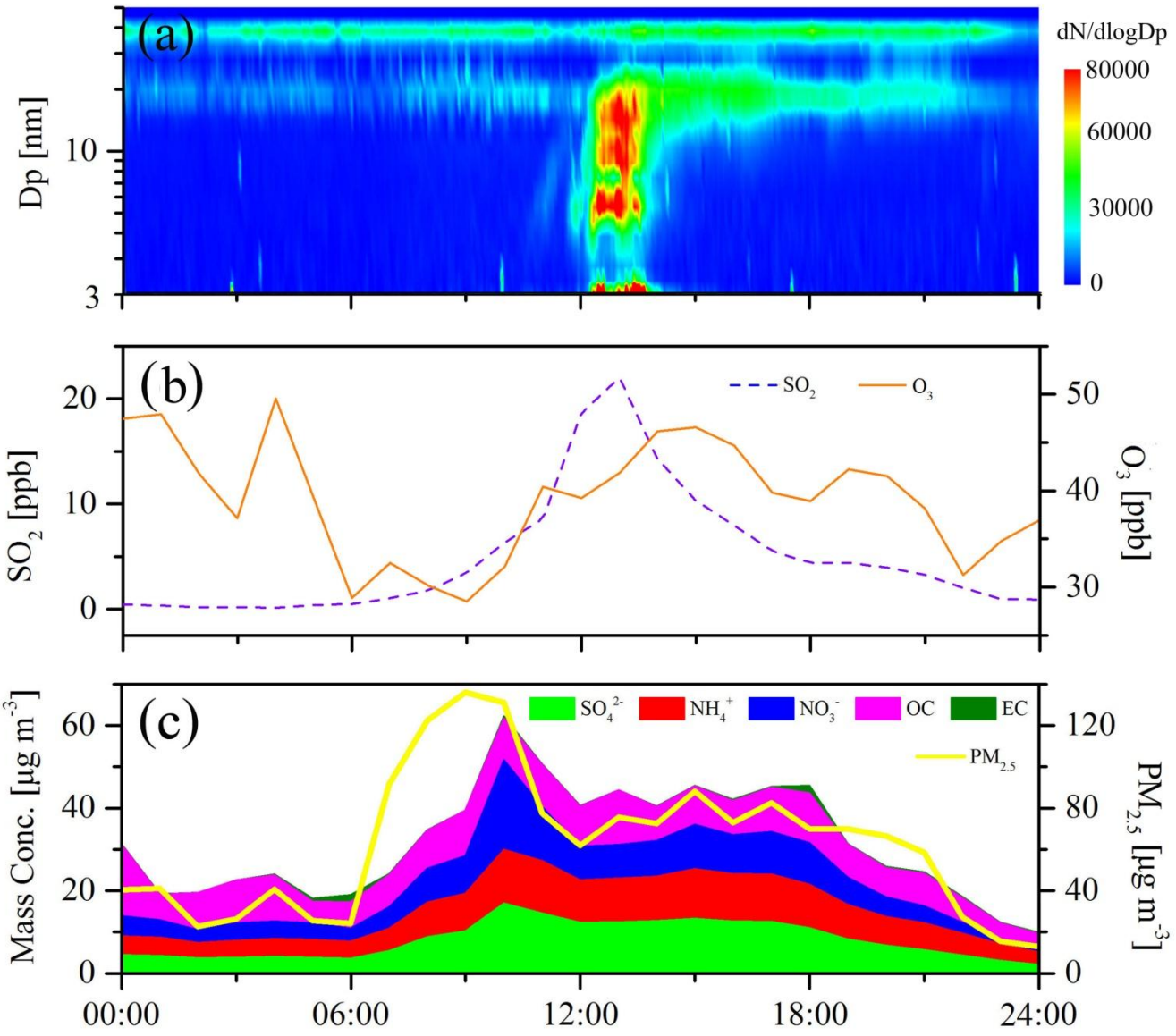

Fig. 7. Time series of particle size distribution, trace gases, chemical composition and mass concentration of $PM_{2.5}$ on 11 November 2014.

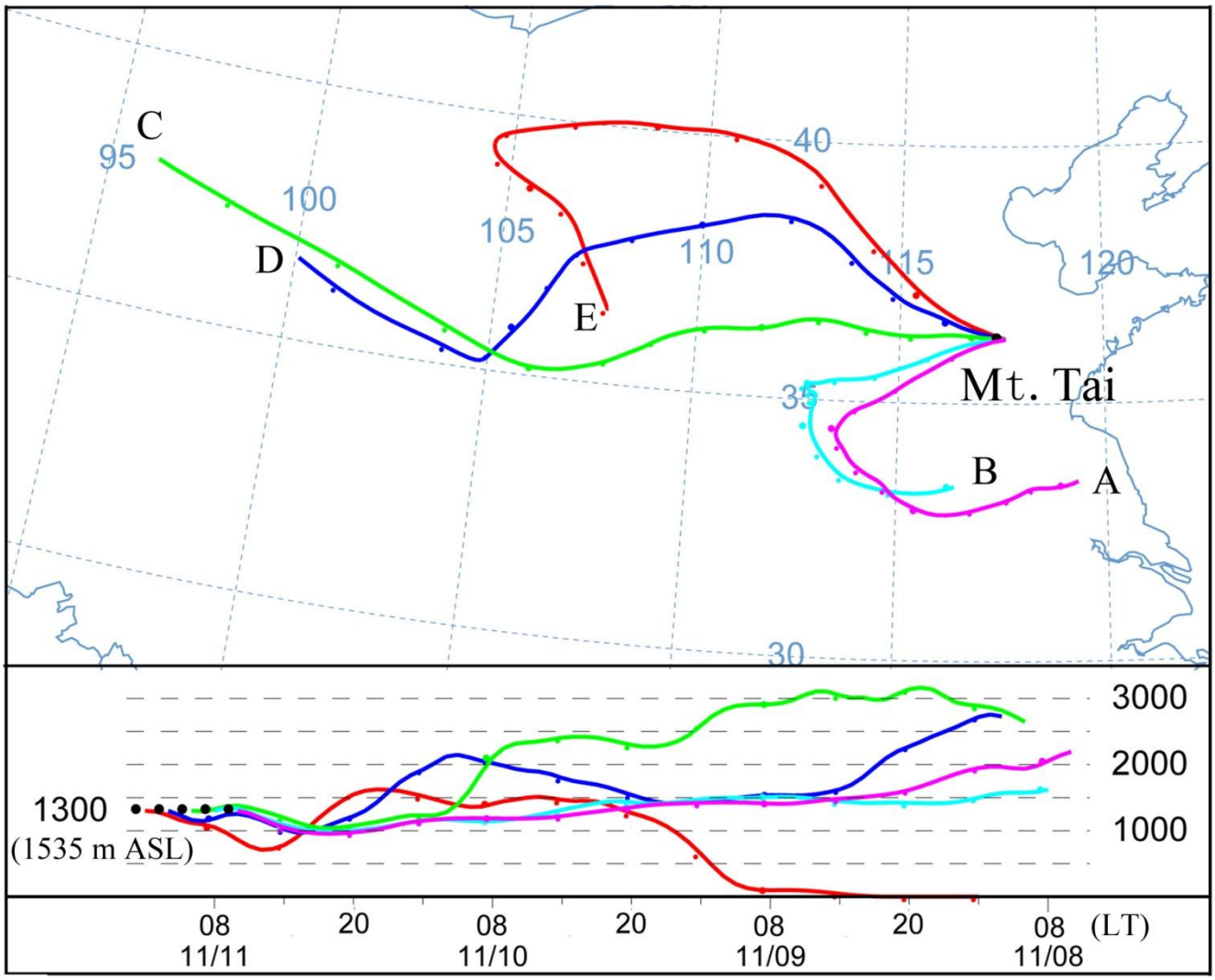

Fig. 8. Air mass backward trajectories for 72 h at 1535 m ASL at 6:00 (A), 8:00 (B), 10:00 (C), 12:00 (D) and 14:00 LT (E) on 11 November 2014.

Table 1. The calculated parameters of all the NPF events during the three campaigns, the minima and maxima are marked in blue and red, respectively

Campaign	Date	J_3 cm^{-3} s^{-1}	$J_{3\text{-}20}$ cm^{-3} s^{-1}	GR $nm\ h^{-1}$	CS 10^{-2} s^{-1}	$[H_2SO_4]$ 10^6 cm^{-3}	SO_2 ppb	O_3 ppb	Date	J_3 cm^{-3} s^{-1}	$J_{3\text{-}20}$ cm^{-3} s^{-1}	GR $nm\ h^{-1}$	CS 10^{-2} s^{-1}	$[H_2SO_4]$ 10^6 cm^{-3}	SO_2 ppb	O_3 ppb
Phase **I**	26-Jul-14	3.34	13.32	1.54	0.5-3.1	N/A	N/A	56±7	8-Aug-14	2.61	16.30	1.15	1.8-15.9	2.87	2.7±2.3	65±10
	27-Jul-14	0.94	6.12	1.55	0.6-2.1	N/A	2.4±2.0	56±9	11-Aug-1	N/A	1.44	1.71	0.2-6.9	3.81	0.6±0.5	56±6
	2-Aug-14	N/A	3.60	3.81	0.1-8.7	N/A	N/A	22±13	12-Aug-1	N/A	40.13	3.69	0.8-7.4	22.1	10.8±7.9	79±16
	3-Aug-14	N/A	1.69	**7.76**	0.1-26.9	N/A	1.5±1.2	35±17	15-Aug-1	2.75	4.52	3.00	N/A	N/A	1.0±1.0	63±12
	6-Aug-14	23.90	52.54	5.78	0.2-1.9	N/A	4.8±2.6	50±5	20-Aug-1	**0.82**	1.33	4.80	0.6-2.7	9.25	5.2±4.3	72±8
	7-Aug-14	N/A	10.90	1.45	0.1-24.8	N/A	1.5±1.7	56±4								
Phase **II**	22-Sep-14	0.99	1.58	1.12	0.7-9.0	7.74	5.7±1.7	76±8	4-Nov-14	7.73	15.06	0.77	0.6-1.5	5.39	6.3±1.2	56±3
	29-Sep-14	16.63	54.97	1.13	0.7-21.1	2.43	1.4±1.1	48±5	6-Nov-14	0.98	**1.10**	1.45	0.1-1.2	2.02	0.6±0.5	13±5
	30-Sep-14	7.94	20.61	1.62	0.5-28.4	1.09	1.9±0.5	2±1	7-Nov-14	1.40	5.59	1.26	0.1-2.0	0.93	0.4±0.3	23±11
	2-Oct-14	5.16	12.02	1.15	0.2-6.6	1.98	1.6±1.7	41±4	8-Nov-14	9.40	13.53	2.95	0.4-2.3	6.71	4.1±2.6	38±3
	3-Oct-14	5.44	14.07	1.50	0.1-4.6	1.34	0.7±0.7	42±3	10-Nov-1	1.02	2.17	3.41	N/A	N/A	2.3±0.7	60±4
	5-Oct-14	8.13	26.41	2.00	0.5-6.9	**0.52**	0.2±0.1	11±5	11-Nov-1	3.29	14.42	2.52	N/A	N/A	7.8±8.3	34±5
	6-Oct-14	2.54	8.94	0.78	0.4-3.4	0.53	0.3±0.4	7±2	12-Nov-1	12.39	26.36	1.09	N/A	N/A	1.6±0.4	35±2
	8-Oct-14	N/A	1.40	0.92	N/A	N/A	5.0±0.6	71±6	14-Nov-1	9.92	13.41	1.55	N/A	N/A	6.1±4.0	40±2
	10-Oct-14	6.54	27.04	1.80	0.2-1.6	4.33	1.8±2.1	54±3	16-Nov-1	5.36	11.06	2.47	0.5-1.2	11.6	5.7±2.9	34±6
	11-Oct-14	9.43	20.37	0.70	0.2-2.2	1.50	3.1±2.5	68±6	17-Nov-1	9.15	16.82	1.10	0.2-0.9	8.38	1.5±0.2	38±2
	13-Oct-14	6.17	26.84	1.64	0.4-2.0	7.43	5.1±1.6	27±8	18-Nov-1	20.45	57.11	0.80	0.1-1.6	4.42	N/A	N/A
	14-Oct-14	10.15	18.11	1.55	0.1-1.4	1.43	0.9±0.8	44±4	19-Nov-1	8.89	15.41	2.51	0.3-2.8	N/A	N/A	N/A
	15-Oct-14	6.76	30.54	2.76	N/A	N/A	10.1±2.9	60±6	22-Nov-1	N/A	11.60	1.23	0.3-5.6	4.18	5.3±4.9	10±8
	16-Oct-14	6.14	36.96	**0.58**	N/A	N/A	1.5±1.9	41±1	24-Nov-1	11.03	24.51	1.50	N/A	N/A	2.9±2.1	26±10
	17-Oct-14	1.55	5.75	2.12	N/A	N/A	N/A	N/A	25-Nov-1	7.11	10.97	2.02	0.1-2.9	N/A	0.5±0.4	25±13
	18-Oct-14	6.16	22.89	2.03	N/A	N/A	N/A	N/A	1-Dec-14	4.96	7.55	1.77	0.1-0.9	1.22	1.4±0.3	27±4
	21-Oct-14	N/A	1.98	2.36	0.4-1.3	N/A	0.3±0.3	13±5	3-Dec-14	**25.04**	**57.43**	1.51	0.4-1.4	1.64	12.9±9.6	13±11
	24-Oct-14	3.64	8.99	1.25	0.5-1.3	1.12	N/A	N/A	4-Dec-14	4.80	10.62	2.69	0.4-1.4	5.48	2.9±0.3	13±9
	25-Oct-14	7.50	14.74	1.60	0.4-1.4	0.89	0.3±0.3	15±11	5-Dec-14	3.34	5.83	1.32	0.2-1.2	0.95	N/A	4±1
	27-Oct-14	7.24	15.49	0.99	N/A	N/A	0.2±0.3	12±4	6-Dec-14	N/A	1.52	1.99	N/A	N/A	2.2±1.2	4±9
	28-Oct-14	2.98	13.17	1.21	N/A	N/A	0.2±0.1	5±2	7-Dec-14	N/A	11.64	1.42	N/A	N/A	7.9±2.5	8±5
	2-Nov-14	11.24	17.78	0.72	0.2-0.9	4.97	0.7±0.1	33±3	8-Dec-14	9.78	16.33	1.24	N/A	N/A	2.4±1.4	16±10
	3-Nov-14	8.77	18.57	1.10	0.3-1.3	6.65	4.6±0.6	37±3								
Phase **III**	16-Jun-15	1.45	9.22	3.98	1.7-4.9	13.6	6.3±0.8	105±7	4-Jul-15	12.55	23.25	0.91	N/A	N/A	5.7±2.9	95±20
	20-Jun-15	6.16	32.50	3.28	0.5-1.8	10.5	2.8±1.6	81±11	8-Jul-15	N/A	8.25	0.93	0.6-2.3	N/A	0.5±0.5	90±16
	21-Jun-15	3.90	6.08	3.44	1.4-3.0	**25.7**	10.0±2.1	105±15	13-Jul-15	N/A	5.64	1.95	1.0-2.4	1.10	0.1±0.1	110±15
	2-Jul-15	9.61	43.41	1.08	0.2-1.9	N/A	2.2±1.3	69±10	15-Jul-15	N/A	19.72	2.86	0.7-1.6	N/A	0.2±0.1	88±12
	3-Jul-15	5.54	10.86	2.65	0.2-2.1	N/A	5.5±2.5	101±13	25-Jul-15	N/A	19.56	1.88	0.4-1.9	2.41	0.3±0.2	99±9

Table 2. Summary of averages, medians, 25th percentiles, 75th percentiles, minima and maxima for the calculated parameters on the basis of Table 1

	Average	Minimum	Maximum	25th percentile	Median	75th percentile
J_3 (cm^{-3} s^{-1})	7.10	0.82	25.04	3.31	6.15	9.41
$J_{3\text{-}20}$ (cm^{-3} s^{-1})	16.61	1.10	57.43	6.12	13.47	20.61
GR ($nm\ h^{-1}$)	1.98	0.58	7.76	1.15	1.55	2.51
CS (10^{-2} s^{-1})	1.4	0.1	28.4	0.5	0.9	1.7
$[H_2SO_4]$ (10^6 cm^{-3})	5.23	0.52	25.7	1.28	3.34	7.07
SO_2 (ppb)	3.2	0.1	12.9	0.7	2.2	2.7
O_3 (ppb)	45	2	110	19	41	66

Table 3. Comparison of NPF characteristics between Mt. Tai and other studies in China

Observation site	FR (cm^{-3} s^{-1})	GR (nm h^{-1})	Freq.	Data	Air mass style	Ref.
Mt. Tai	7.10±5.39 (J_3)	1.98±1.27 (GR_{3-20})	40 %	Jul-Dec 2014 & Jun-Aug 2015	Mountain (1534 m ASL)	This study
Mt. Tai Mo Shan	0.97-10.2 ($J_{5.5}$)	1.5-8.4 ($GR_{5.5-25}$)	33 %	Oct-Nov 2010	Mountain (640 m ASL)	Guo et al. (2012)
Mt. Huang	0.09-0.30 (J_{10})	1.42-4.53 (GR_{10-20})	37 %	Apr-Jul 2008	Mountain (1840 m ASL)	Zhang et al. (2016)
Mt. Huang		2.29-4.27 (GR_{10-15})	18 %	Sep-Oct 2012	Mountain (869 m ASL)	Hao et al. (2015)
Mt. Daban		0.8-3.2	79 %	Sep-Oct 2013	Mountain (3295 m ASL)	Du et al. (2015)
SouthYellow Sea & East China Sea	0.3-15.2 ($J_{5.6-30}$)	2.5-5.0	16 %	Oct-Nov 2011 & Nov 2012	Marine	Liu et al. (2014)
Backgarden	2.4-4.0 (J_{3-25})	4.0-22.7 (GR_{3-25})	25 %	Jul 2006	Rural	Yue et al. (2013)
Nanjing	2.6 (J_6)	10.4 (GR_{6-30})	44 %	Dec 2011-Nov 2013	Suburban	Qi et al. (2015)
Lanzhou		1.2-16.9 (GR_{10-20})	33 %	Jun-Jul 2006	Suburban	Gao et al. (2012)
Xinken	0.5-5.2 (J_{3-20})	2.2-19.8 (GR_{3-20})	26 %	Oct-Nov 2004	Suburban	Liu et al. (2008)
Shanghai	2.3-19.2 (J_3)	1.9-38.3 (GR_{7-20})	21 %	Nov 2013-Jan 2014	Urban	Xiao et al. (2015)
Nanjing	1.6-6.7 (J_{10-25})	5.6-9.6 (GR_{10-25})	40 %	Jul-Aug 2012	Urban	An et al. (2015)
Beijing	5.0-44.9 (J_3)	1.86-6.7 (GR_{7-30})	26 %	Jul-Sep 2008	Urban	Wang et al. (2015)
Lanzhou	0.2-6.2 ($J_{14.6-25}$)	2.6-12.3 ($GR_{14.6-25}$)	34 %	Aug-Nov 2014	Urban	Zhang et al. (2017)
Qingdao	13.3 ($J_{5.6-30}$)	2.0-10.2	41 %	Apr-May 2010	Urban	Zhu et al. (2014)
Hong Kong	1.9 ($J_{5.5}$)	3.7-8.3 ($GR_{5.5-10}$)	23 %	Dec 2010-Jan 2011	Urban	Wang et al. (2014a)